Phase transition and flow-rate behavior of merging granular flows

Mao-Bin Hu,[1,*] Qi-Yi Liu,[1] Rui Jiang,[1,2] Meiying Hou,[3,†] and Qing-Song Wu[1]

[1]*School of Engineering Science, University of Science and Technology of China, Hefei 230026, P. R. China*

[2]*MOE Key Laboratory for Urban Transportation Complex Systems Theory and Technology, Beijing Jiaotong University, Beijing 100044, P. R. China*

[3]*Beijing National Laboratory for Condensed Matter Physics and CAS Key Laboratory of Soft Matter Physics, Institute of Physics, Chinese Academy of Sciences, Beijing 100190, China*

(Received 30 October 2014; revised manuscript received 28 January 2015; published 18 February 2015)

Merging of granular flows is ubiquitous in industrial, mining, and geological processes. However, its behavior remains poorly understood. This paper studies the phase transition and flow-rate behavior of two granular flows merging into one channel. When the main channel is wider than the side channel, the system shows a remarkable two-sudden-drops phenomenon in the outflow rate when gradually increasing the main inflow. When gradually decreasing the main inflow, the system shows obvious hysteresis phenomenon. We study the flow-rate-drop phenomenon by measuring the area fraction and the mean velocity at the merging point. The phase diagram of the system is also presented to understand the occurrence of the phenomenon. We find that the dilute-to-dense transition occurs when the area fraction of particles at the joint point exceeds a critical value $\phi_c = 0.65 \pm 0.03$.

DOI: 10.1103/PhysRevE.91.022206 PACS number(s): 45.70.−n, 52.77.−j, 89.75.Fb

I. INTRODUCTION

Granular materials are ubiquitous in natural, industrial, mining, and geological processes. While they are comprised of many particles, their bulk properties exhibit many nonlinear phenomena such as force chains [1], solitons [2], surface waves [3,4], resistance to penetration [5], mixing and segregation [6,7], jamming and clogging [8–11], granular flow [12–14], granular clock [15,16], etc. Dynamic behavior of granular flow is one of the most challenging subjects in this field [17,18]. The granular flow can be normally classified into three states: dilute flow, dense flow, and jammed, where the grains behave like gas, liquid, and solid, respectively. Transitions among the three states have attracted intensive interests. For example, To *et al.* studied the jamming phenomenon of granular flow in a hopper and found the transition depends on d/d_0, where d is exit width and d_0 is particle diameter [8]. Thomas and Durian studied the clogging phase diagram as a function of aperture size and tilting angle [9]. Chen *et al.* studied dilute and dense granular flows down a pipe with an electric field [12]. In dense flow state, the flow rate depends only on the exit size d and the particle diameter d_0. Beverloo *et al.* found an empirical relation $F \sim (d - kd_0)^{\alpha}$ by dimensional analysis [19]. Janda *et al.* studied the velocity and density profiles of granular flow through an aperture and derived a remarkable expression for the outflow with clear physical meanings for all terms [20,21]. Hou *et al.* found the critical flow rate q_c for dilute-dense transition scales as a function of $\frac{d}{d_0}\frac{d}{(D-d)}$, rather than d/d_0, where D is channel width [13]. Many nonlinear phenomena have been revealed in granular flow. For example, in dense granular flow, the particle velocity shows three classes of distributions [22]. On a bumpy inclined plane, steady granular flow can be obtained only in a narrow range of angles [23]. On an inclined plane, disordered-to-ordered flow transition is observed when changing the basal roughness [24]. In a channel with two successive bottlenecks, a bistable phenomenon of dilute and dense flow state is discovered when the channel width is properly adjusted [25,26].

In real processes of granular materials, there are often joint points where granular flows merge and interact. However, effects of merging granular flow are still poorly understood. Recently, Yang *et al.* found a boundary shock phase for merging system [27]. In this paper, we focus on the dilute-dense transition and flow-rate features of merging granular flow. We study a merging system with two channels, each fitted with a gate to control the inflow rates. Although this is reminiscent of the on-ramp system in vehicular traffic [28–30], the granular merging system shows remarkably new features in the phase transition and flow-rate behavior. In the traffic flow system, three distinct dynamic phases are observed on highways: the free traffic flow, the traffic jam (which is a localized region of very high density where vehicles either cannot move at all or where every vehicle comes to a brief stop), and the synchronized traffic flow (in which vehicles are in congestion but with no significant stoppage). Recent experimental investigation shows that in the majority of cases, synchronized traffic is observed localized near bottlenecks and thus bottlenecks are important for the formation of synchronized traffic. Among the various types of bottlenecks, the on-ramp is of particular interest to researchers and has been widely studied.

In our experiment of granular merging flow, when the main channel is wider than the side channel, an interesting two-sudden-drops phenomenon in the outflow rate is observed. Moreover, the system's outflow behavior shows obvious hysteresis. We adopt the method of particle tracking to find the area fraction and the mean velocity of particles to quantitatively analyze the reason for flow-rate drop. Varying the gate width from the merging channels, the system shows four states: LL, LH, HL, and HH, where L stands for dilute flow (low density), H stands for dense flow (high density), and LL, LH, HL, HH stand for the flow states of the two channels. The phase diagram of the system is also presented. Finally, we find that the dilute-dense transition occurs when the area

*humaobin@ustc.edu.cn

†mayhou@iphy.ac.cn

fraction of particles at the joint point exceeds a critical value $\phi_c = 0.65 \pm 0.03$.

II. EXPERIMENTAL SETUP

The experiments are carried out in a quasi-two-dimensional channel system. The channel is established with specially shaped glass spacers between a metal base and a glass cover plate. The whole system is mounted on a platform with an angle of 30° to the horizon (see Fig. 1). The gap between the base and the cover plate is kept at 3.0 mm to ensure a single-layer flow of stainless steel beads with diameter $d_0 = 2.5 \pm 0.001$ mm. The mass of a single steel bead is about 0.06 g. The channels are designed as follows. Two channels (A and B) share the same granular bead reservoir (top hopper). The channels have different widths of D_A and D_B, respectively. The inflow of each channel is controlled by a gate. The gate widths (D_1 for channel A, and D_2 for channel B) are adjustable to control the inflow rates. Granular flows from the two channels merge at point M. The final channel (below M) has the width of D_A. Because channel A is straight while channel B has a turning, we call channel A the main channel, and call channel B the side channel. In the following discussion, the main channel has width $D_A = 40$ mm and the side channel has width $D_B = 30$ mm unless stated otherwise. Note that the width of the side channel at the turning point is enlarged to 40 mm, so that the top channel gate is the only bottleneck along the side channel. This is to avoid the two bottleneck interactions in the side channel [25].

Before each run of experiment, the gate widths are set to some values. In most of the experiments, the reservoir and the channels are initially empty (without particles), unless otherwise mentioned. This is equivalent to the case of dilute-to-dense transition when gradually opening the gate. Then, the steel beads are poured into the top reservoir and granular flows are initiated instantaneously by gravity in both channels. At the final exit, the total mass of the beads falling out of the system is measured by an electronic balance with the sensitivity of 0.1 g and the weighing period of 0.2 s. Then, the outflow rate $J(t)$ is obtained by calculating the slope of the recorded mass data. The outflow rate data in the figures are typically averaged over 10 granular flow experiments. A high speed camera (480fps) is adopted to capture the flowing state at the merging point M. The area fraction of particles and the average velocity of particles are estimated based on the captured videos by a particle tracking software. The box for determining the area fraction and the line for determining the velocity are depicted in Fig. 1(c). This is similar to that described in Janda *et al.*'s previous work [20].

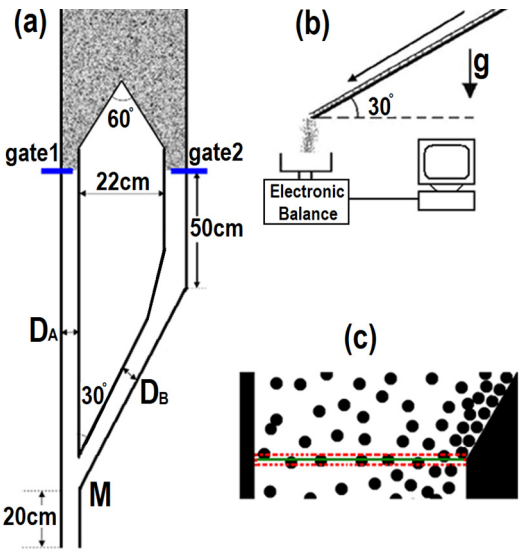

FIG. 1. (Color online) (a) Top view and (b) side view of the granular merging flow channels. (c) Red box and green line show the positions where the area fraction and mean velocity are determined.

When the particle density is very low, we find that the typical velocities of particles at point M are $V_A \approx 1.5 \pm 0.2$ m/s for channel A, and $V_B \approx 1.0 \pm 0.2$ m/s for channel B. Because channel B has a turning, particles in it will collide more frequently with the sidewalls. As a result, the mean velocity of particles in channel B is relatively lower. At point M where two granular flows merge, the mean velocity is greatly reduced because of collisions. This behavior strongly affects the flow rate of the system, which will be discussed in detail.

III. EXPERIMENT RESULTS

The phase transition and the flow-rate behavior are the most intriguing phenomena in a granular merging system. By varying the gate widths of the channels (D_1 and D_2), the granular flow in the channels can be dilute flow (low density) or dense flow (high density). For simplicity, we denote dilute flow as L, and dense flow as H. Here, we use area fraction of particles in the channel to determine the dilute flow state and the dense flow state. For the dilute flow state, the area fraction in the channel is below $\phi_c = 0.65$. For the dense flow state, the area fraction is above ϕ_c. Here, $\phi_c = 0.65$ is the critical area fraction of dilute-to-dense transition. The reason for ϕ_c will be explained later. The flow state can be also determined by the variation of its final inflow rate F_∞ with respect to its initial inflow rate F_0 at the beginning of experiment, similar to the common practice in vehicular traffic congestion studies [29,30]. If the final inflow rate is the same as the initial inflow rate, i.e., $F_\infty = F_0$, the flow is dilute. If the final inflow rate is lower than the initial inflow rate, i.e., $F_\infty < F_0$, the flow is dense. The results are the same with the area fraction criterion and with the flow-rate criterion.

Figure 2 shows the four typical granular flow states. LL: both channels are dilute. LH: channel A is dilute while channel B is dense. HL: channel A is dense while channel B is dilute. HH: both channels are dense.

We first measure the variation of inflow rates with gate width D_1 or D_2 for the channels, respectively, as shown in Fig. 3. When measuring the inflow rate of the main channel, the side channel gate is completely closed, and vice versa. Because the granular flow is always dense above the gates, the inflow rate will only depend on the gate width [19–21]. One can see that the inflow rates increase with gate width and can be fitted by Beverloo *et al.*'s empirical equation [19]

$$F = C_1(D - kd_0)^{n+1/2} + F_0 \tag{1}$$

or by Janda *et al.*'s new expression [20]

$$F = C_2(1 - 0.5e^{-R/3.3})R^{n+1/2}, \tag{2}$$

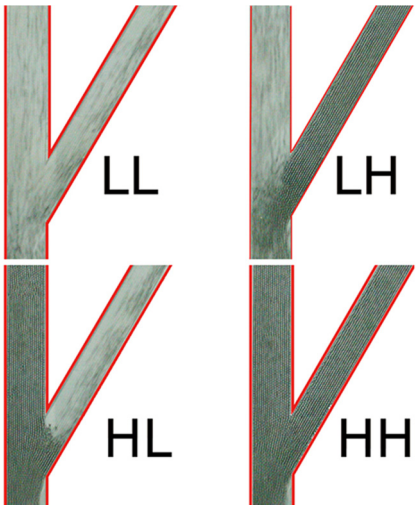

FIG. 2. (Color online) Snapshots of typical granular flow patterns. (a) LL state ($D_1 = 20$ mm, $D_2 = 20$ mm); (b) LH state ($D_1 = 30$ mm, $D_2 = 30$ mm); (c) HL state ($D_1 = 40$ mm, $D_2 = 18$ mm); (d) HH state ($D_1 = 40$ mm, $D_2 = 25$ mm).

where D is the gate width ($D = D_1$ or $D = D_2$), $R = D/2$, $d_0 = 2.5$ mm is the particle diameter, C_1 is equivalent to $C\rho_b\sqrt{g}$ in a typical Beverloo's equation [19], C_2 is equivalent to $C''\sqrt{g}\phi_\infty$ in Janda's original expression [20], $n = 1$ ($n = 2$) for the two-dimensional (3D) case. Here, we have $n = 1$. The fitting results are $C_1 = 1.0$ g/s, $k = 4$, $F_0 = 19.0$ g/s, and $C_2 = 1.3$ g/s. We note that the Beverloo's fit needs an additional flow of F_0. The term of F_0 is necessary because the initial flow rate at $D = 4d_0$ is not zero. At $D = 4d_0$, the granular flow has a high probability to clog. If clogged, the flow rate is zero. If the flow is not clogged, the flow rate is $F_0 = 19.0$ g/s. Therefore, Janda's equation fits better than the Beverloo one.

Then, we study the outflow rate with a fixed $D_2 = 30$ mm and varying D_1, that is, the side gate is completely opened

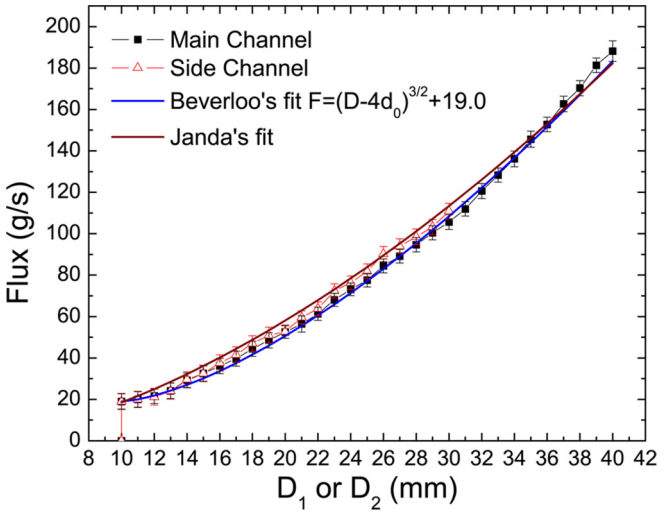

FIG. 3. (Color online) Inflow rate from the channels vs channel gate width D_1 or D_2. The flow rate is fitted with the Beverloo's fit and the Janda's fit as formulated by Eqs. (1) and (2). Data are obtained by averaging the results of 10 independent experiments.

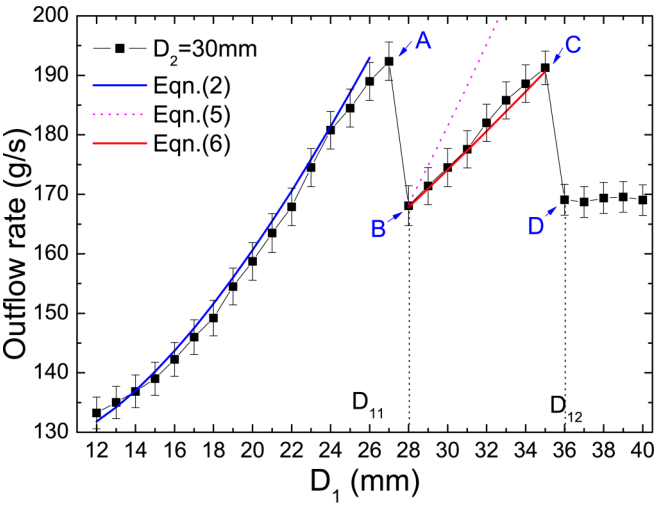

FIG. 4. (Color online) Outflow rate vs main channel gate width D_1, with fixed $D_2 = 30$ mm and initially empty channels. The two vertical dotted lines are guides for the phase transition points. Data are obtained by averaging the results of 10 independent experiments.

while the main gate is gradually opened. Figure 4 shows the variation of outflow rate with D_1. When $D_1 \leqslant 27$ mm, the granular flows in both channels are dilute. One can see that the outflow rate increases with D_1 and can be fitted with

$$F = F_A + F_B \approx (D_1 - 4d_0)^{3/2} + 128.0, \tag{3}$$

where F_A is the inflow rate from the main channel and is estimated by Eqs. (1) and (2), F_B is the inflow rate from the side channel (here $F_B = F_{B\max} \approx 109.0$ g/s). Interestingly, when $D_1 > 27$ mm, there are two sudden drops in the outflow rate. The two drops correspond to the dilute-to-dense transition in the side channel (LL to LH) at $D_{11} = 27$ mm, and then the dilute-to-dense transition in the main channel (LH to HH) at $D_{12} = 35$ mm. In Fig. 4, we use four points (A, B, C and D) to mark the critical points of transition: (A) the last LL state; (B) the LL-LH transition point; (C) the last LH state; (D) the LH-HH transition point. In the following, we will show the detail observations at the four points.

(A) $D_1 = 27$ mm, the last LL state. In the LL state, although both channels are dilute, the granular flow from the side channel (the side flow) collides with the granular flow in the main channel (the main flow) and increases the granular density at the merging point M. As a result, the side flow acts like a "soft obstacle" for the main flow. Increasing the inflow, the size of the soft obstacle will increase and finally block the whole merging area, and the dilute-dense transition will occur. At $D_1 = 27$ mm, the area fraction of particles at the joint point M reaches a critical value near $\phi_c = 0.65 \pm 0.03$. This critical density is in agreement with the literature (Hou *et al.* [13]). If the area fraction exceeds ϕ_c, the dilute-to-dense transition will occur. The outflow rate can be estimated by the following equation:

$$F = \rho V D = \left(\frac{\phi m_0}{S_0}\right) V D, \tag{4}$$

where ρ is granular density, $S_0 \approx 4.9 \times 10^{-6}$ m^2, and $m_0 \approx 0.06$ g are the area and the mass of one steel bead, ϕ and V are the area fraction and the mean velocity of

particles at point M, D is exit width, respectively. At $D_1 = 27$ mm, we find that the mean velocity of particles at M is $V \approx 0.62 \pm 0.1$ m/s. This indicates that the particles' velocity is greatly reduced due to the interaction of granular flows. The area fraction is near $\phi \approx 0.63$ and the exit width is $D = D_A = 40$ mm. With Eq. (4), we get $F \approx 191$ g/s. This is close to the experiment result of 192 g/s.

(B) $D_1 = 28$ mm, the LL-LH transition point. The dilute-to-dense transition process is described as follows. In the first moment of flowing, both channels are dilute. The mean area fraction at the merging point M will increase rapidly and slightly exceed the critical value of 0.65. But, the flow with high density and high velocity can only sustain for a very short moment. Then, the dilute-to-dense transition happens at point M. The area fraction at point M drops to around 0.58 ± 0.03. Meanwhile, the mean velocity also decreases to about 0.59 m/s. After the transition, the dense flow front will propagate upward to the side channel because the granular density in side channel is higher than the main channel. The main channel remains dilute. By Eq. (4), we get the flow rate $F \approx 168$ g/s, in agreement with measurement.

After the side flow becomes dense, we can also measure the area fraction and the mean velocity of the dense granular flow at the upper straight section of channel B. We find that the area fraction in the side channel is $\phi \approx 0.75 \pm 0.03$, while the mean velocity is 0.27 ± 0.05 m/s (note that both values are measured at the upper straight section of the side channel, different from point M). One can get $F_B \approx 74$ g/s by using Eq. (4) with $D_B = 30$ mm. On the other hand, because the main channel is dilute, we can get $F_A \approx 95$ g/s by Eqs. (1) or (2) with $D_1 = 28$ mm. The total outflow is the sum of F_A and F_B, that is, 169 g/s. This is close to the experiment result. In the experiment, we find that the area fraction of dense granular flow at the upper straight section of the channel is $\phi \approx 0.75 \pm 0.03$. This value is higher than the area fraction at the merging point M, but it is below the critical area fraction of two-dimensional (2D) jamming transition ($\phi \approx 0.84$). In the upper straight part of the densely flowing channel, the particles automatically form many vertical chains moving downward in parallel, while the triangular and honeycomb-alike structures are rarely observed. One can estimate that the area fraction for the chainlike packing structure should be $\phi_d \approx \pi R^2/4R^2 \approx 0.78$. This is close to our observation.

(C) $D_1 = 35$ mm, the last LH state. In the LH state, the right part of the merging area is dense, while the left part remains dilute (see Fig. 2). The side flow acts like a "soft obstacle" for the main flow. However, the overall area fraction is below $\phi_c \approx 0.65$ at the merging area M. Increasing the main flow, the size of the soft obstacle will increase and block the whole merging area, until it triggers the dilute-dense transition again. At point C, we find that the area fraction is near $\phi \approx 0.63$ and the mean velocity is $V = 0.62 \pm 0.1$ m/s. Similarly, the maximal flow rate is $F_c \approx 191$ g/s by Eq. (4), which agrees with the measured result. One can see that the outflow rates are equal for points A and C. At the two points, the average area fraction and the mean velocity are similar at the merging point. Therefore, at both points, the system has reached the same maximal outflow rate.

(D) $D_1 = 36$ mm, the LH-HH transition point. At the beginning of flowing, because both channels are dilute, the area fraction at point M will rapidly increase and exceed 0.65. Then, the area fraction will drop because the dilute-to-dense transition happens. Under the condition, the dense flow front will propagate to both channels and produce a HH state. After the HH state is reached, we find that the mean area fraction is 0.58 ± 0.03 and the mean velocity is 0.59 ± 0.1 m/s at merging point M. With $D = 40$ mm, we get $F \approx 168$ g/s by Eq. (4). This agrees with the experiment result. One can see that the outflow rates are equal for points B and D because the system has reached its dense flow rate of the merging flow bottleneck.

When $D_1 \geqslant 36$ mm, one might think the outflow rate can be estimated by Eqs. (1) or (2) because the flows are dense and the outflow is controlled by the exit width at point M. We get $F = 183$ g/s with width $D_A = 40$ mm by Eq. (1). This is higher than experiment (168.0 g/s). This discrepancy is because of the influence of side channel on main channel. In the HH states (see Fig. 2), there is a vacant area at the lower right of merging area. It is formed due to the intervention of the side flow. The vacant area decreases the efficient exit width and leads to a lower outflow rate.

When $D_{11} < D_1 < D_{12}$, the outflow rate increases monotonically with D_1. One might think that the inflow rate from side channel F_B keeps constant, while F_A increases. This postulation will come to a prediction of outflow rate with the following form (as shown in Fig. 4 with the pink dotted line):

$$F = F_A + F_B \approx (D_1 - 4d_0)^{3/2} + 92.0. \tag{5}$$

However, the experiment results deviate from this prediction. The flow rates show a different scaling behavior with exponent 1.3 (as shown in Fig. 4 with the red solid line):

$$F \approx (D_1 - 4d_0)^{1.3} + 125.0. \tag{6}$$

Compared with Eq. (5), this outflow rate is relatively smaller. This implies that when $D_{11} < D_1 < D_{12}$, the inflow rate from side channel actually decreases with D_1. This is because the main channel flow hinders the side channel flow. The larger the main channel inflow, the greater the side channel flow is hindered. Therefore, the inflow rate from side channel decreases with D_1.

In Fig. 5, we show the evolutions of the area fraction ϕ and the mean velocity V with main channel gate width D_1. Note that both values are measured at the merging point M after the flows reach a steady state. That is, the first 10 s of the flowing are not considered. For the LL state, ϕ increases with D_1 while V decreases with D_1. For the LH state, both ϕ and V increase with D_1. For the HH state, both ϕ and V are almost constant.

Then, we study the hysteresis behavior of the system. Figures 4 and 5 show the result with initially empty channels. This is equivalent to the case of gradually increasing gate width D_1. Figure 6 shows the variation of outflow rate with D_1 when the channels are initially full of particles. This is equivalent to the case of gradually decreasing gate width D_1. One can see that the system shows HH, LH, and LL states. But, the transition points are lower than those in Fig. 4. For the LL and HH states, the flow rate is the same as in Fig. 4. In the LH state, the flow rate decreases monotonically with D_1. Moreover, there are no flow-rate jumps for the HH-LH and LH-HH transitions. Obviously, the system shows hysteresis in the path of increasing and then decreasing D_1. For the cases in Fig. 6, we find that the mean area fraction at the merging point

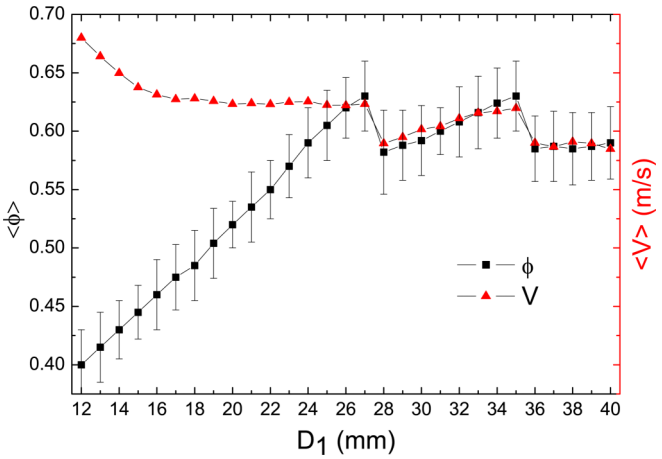

FIG. 5. (Color online) Evolutions of the area fraction ϕ (solid squares) and the mean velocity V (solid triangles) with main channel gate width D_1. Here, the side channel gate width D_2 remains at 30 mm. The standard deviation of V is about 0.1.

M never increases to above 0.62 throughout the process, while the mean velocity decreases monotonically with decreasing D_1. As a result, the outflow decreases monotonically with D_1.

To better understand the merging behavior, we present the phase diagrams of the merging flow system in Fig. 7. Figure 7(a) shows the system's phase diagram with initially empty channels. One can see that the phase diagram consists of four regions: LL, LH, HL, and HH. When the inflow rates from both channels are small, the system is in the LL state. When the inflow rates increase, either of the two channels can transit to dense flow. When the inflow rates are high enough, the system enters the HH state, so that both channels are dense. From Fig. 7(a), one can see that the two-sudden-drops phenomenon will appear when the system undergoes LL-LH and LH-HH transitions. In experiment, we can observe the two-sudden-drops phenomenon with $D_2 \geqslant 20$ mm. If we decrease the gate width of D_2 to below 20 mm, the two-sudden-drops phenomenon will vanish. Figure 7(b) shows the phase diagram

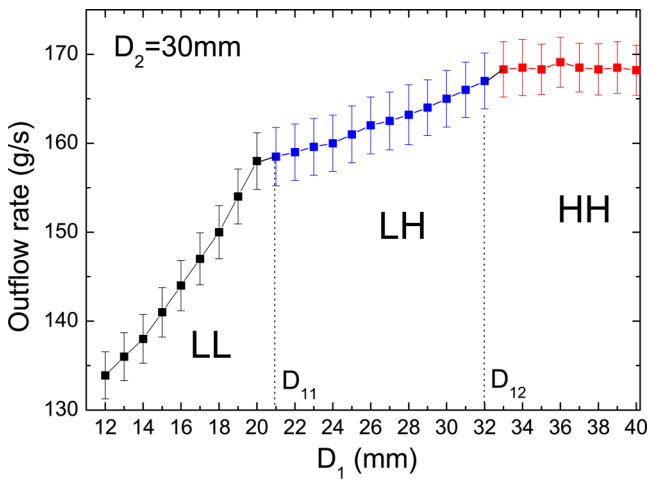

FIG. 6. (Color online) Outflow rate vs main channel gate width D_1, with fixed $D_2 = 30$ mm and initially full channels. The two vertical dotted lines are guides for the phase transition points.

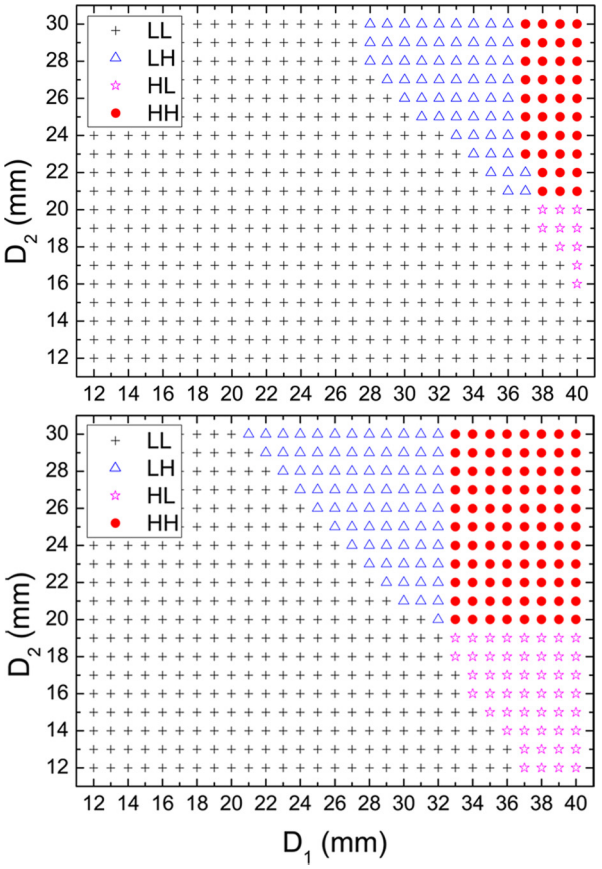

FIG. 7. (Color online) Phase diagrams of the system: (a) initially empty channels; (b) initially full channels. For most data points, we have done several independent granular flow experiments. The first 60 s of experiment is regarded as the transient. For the data at the boundaries, we have done 10 experiments of 5 min to make sure the granular flow is not a transient state.

of the system when the channels are initially full of particles. That is, in each experiment, the channels and the reservoir are all filled with the particles and then the granular flows are initiated by gravity. From Fig. 7(b), we can see that the HH, HL, and LH states occupied bigger areas than in Fig. 7(a). The phase diagram of Fig. 7(a) represents the dilute-to-dense transition, while here Fig. 7(b) represents dense-to-dilute transition. The difference between the two phase diagrams is consistent with the hysteresis behavior of Figs. 4 and 6.

Now, we show the outflow rate with a fixed $D_1 = 40$ mm and a increasing D_2, that is, the main channel is completely opened and then the side channel is opened gradually. Figure 8 shows the variation of outflow rate with initially empty channels. From the phase diagram of Fig. 7(a), there are two phase transitions (LL-HL, and HL-HH) when increasing D_2. However, there is only one sudden drop in the outflow rate at $D_{21} = 15$ mm, corresponding to the LL-HL transition. When the system is in the HL state, there is no obvious increment of outflow rate, and the two-sudden-drops phenomenon does not appear under these conditions. This is different from the LH state. The phenomenon can be explained by the different flow patterns of LH and HL states. As shown in Fig. 9, for the LH state, the left part of the merging area remains dilute because

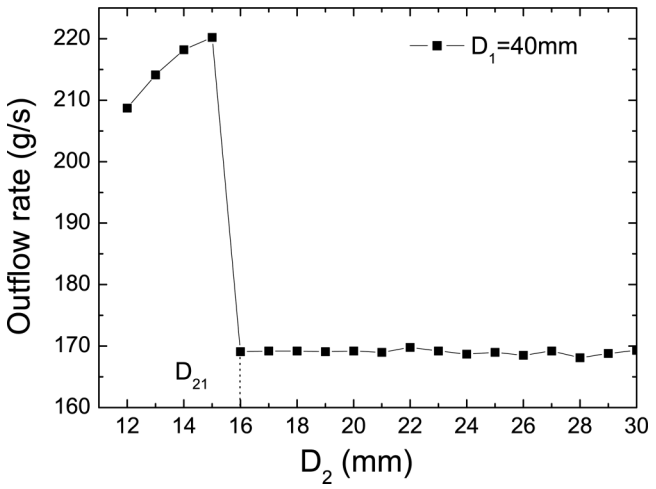

FIG. 8. Outflow rate vs side channel gate width D_2, with fixed $D_1 = 40$ mm. The dotted line is guide for the phase transition point.

the dense flow from the side channel can not affect the whole merging area. Therefore, the flow rate in the main channel can increase with D_1, leading to an increasing outflow rate. However, in the HL state, the whole merging region is dense, as also shown in Fig. 2. Although the inflow rate from the side channel increases with D_2, the inflow rate from the main channel will decrease simultaneously. In this case, the system has reached its dense flow rate. As a result, there is no outflow rate drop for the HL-HH transition, and the two-sudden-drops phenomenon will not appear.

Moreover, in Fig. 8, the maximal outflow rate can reach $F_c \approx 220$ g/s at $D_{21} = 15$ mm. This is higher than the maximal outflow rate of $F_c \approx 192$ g/s in Fig. 4. The difference in maximal outflow rate can be explained as follows. As Eq. (4), the maximal flow rate depends on the product of the critical area fraction, the mean velocity, and the channel width. We find that the critical fraction keeps at $\phi_c \approx 0.65$. But, the mean velocity at the merging point M has a higher value of $V \approx 0.7 \pm 0.1$ m/s. This is because the particle velocity is now dominated by the main channel inflow, which has a higher incoming velocity. Thus, the maximal flow rate is now higher. By Eq. (4), we get $F_c \approx 222$ g/s, which is close to the measured value. Here, one can draw a clue to optimize the flow rate of the system. When two channels merge, it is better to completely open the channel with higher incoming velocity and then gradually open another channel. With the fixed channel widths, if the channel with higher incoming velocity is completely opened and then the other channel is opened gradually, the maximal outflow rate will be higher. In our case, the side channel has a lower incoming velocity because it is with a turning. So, the side channel should be opened gradually after the main channel is completely opened.

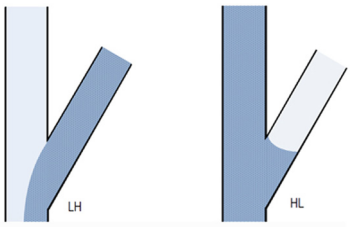

FIG. 9. (Color online) Illustration of the LH state and the HL state. The dark gray area is with high density. The light gray area is with low density. Note that the whole merging area is dense in the HL state.

Finally, we briefly report the experiment results with smaller main channel width of D_A. We find that the two-sudden-drops phenomenon shows only when the main channel is wider than the side channel. When $D_A < D_B$, the dense flow from the side channel will block the whole merging area for the LH state. Therefore, the outflow rate will not increase with D_1 in the LH state. Thus, the two-sudden-drops phenomenon will disappear. In Janda *et al.*'s recent work, they found that the density profile showed substantial decrement when the exit size decreased [20]. As we measure the area fraction at the cross section of the merging point, a similar phenomenon appears. We find that the critical area fraction decreases slightly from $\phi_c = 0.65 \pm 0.03$ to 0.63 ± 0.03 when the exit width decreases from $D_A = 40$ to 20 mm. This phenomenon is in qualitative agreement with the result of Janda *et al.* We have also done experiments when the angle of two channels is 45° and/or 60°. The phase diagrams are also composed of LL, LH, HL, and HH states.

IV. CONCLUSION

In summary, the phase transition and the flow-rate behavior of a merging granular flow system are studied. Although the system shows four flowing states (LL, LH, HL, and HH) similar to the vehicular on-ramp system, some remarkable features are discovered. When gradually opening the main gate, a two-sudden-drops phenomenon in the outflow rate is observed when the main channel is wider than the side channel. The two-sudden-drops phenomenon emerges when the system undergoes a LL-LH transition followed by a LH-HH transition. On the other hand, when the system undergoes LL-HL and HL-HH transitions, there is no two-sudden-drops phenomenon. The system also shows obvious hysteresis when we gradually close the channel gate. To explain the flow-rate-drop phenomenon, we measure the area fraction and the mean velocity at the merging point M. We find a critical area fraction $\phi_c = 0.65 \pm 0.03$ for the occurrence of dilute-to-dense transition. At the dilute-to-dense transition, the area fraction first increases to ϕ_c and then decreases to a lower value. The mean velocity also drops. Therefore, the outflow rate shows a sudden drop.

In this study, the interactions among grains are collision and friction. A similar study to characterize the flow in systems of soft grains, or in which a more viscous interstitial fluid is introduced, would be valuable. The studies can be useful for the efficient transport and processing of granular materials in industry, chemistry, and agriculture. The results may also shed some light on the understanding of molecular motors, colloids, emulsion flow, vehicular traffic flow, and pedestrian flow.

ACKNOWLEDGMENTS

We thank W.-P. Sun for experiment assistance. This work is funded by the National Natural Science Foundation of China with a Key Project No. 11034010 and a Project No. 71171185.

[1] T. S. Majmudar and R. P. Behringer, Nature (London) **435**, 1079 (2005).
[2] P. B. Umbanhowar, F. Melo, and H. L. Swinney, Nature (London) **382**, 793 (1996).
[3] T. Shinbrot and F. J. Muzzio, Nature (London) **410**, 251 (2001).
[4] H. J. van Gerner, M. A. van der Hoef, D. van der Meer, and K. van der Weele, Phys. Rev. E **82**, 012301 (2010).
[5] H. Katsuragi and D. J. Durian, Phys. Rev. E **87**, 052208 (2013).
[6] M. Halidan, G. R. Chandratilleke, S. L. I. Chan, A. B. Yu, and J. Bridgwater, Chem. Eng. Sci. **120**, 37 (2014).
[7] E. Opsomer, N. Vandewalle, M. Noirhomme, and F. Ludewig, Euro. Phys. J. E **37**, 115 (2014).
[8] K. To, P. Y. Lai, and H. K. Pak, Phys. Rev. Lett. **86**, 71 (2001).
[9] C. C. Thomas and D. J. Durian, Phys. Rev. E **87**, 052201 (2013).
[10] C. C. Kuo and M. Dennin, Phys. Rev. E **87**, 030201(R) (2013).
[11] D. Bi, J. Zhang, B. Chakraborty, and R. P. Behringer, Nature (London) **480**, 355 (2011).
[12] W. Chen, M. Hou, K. Lu, Z. Jiang, and L. Lam, Phys. Rev. E **64**, 061305 (2001).
[13] M. Hou, W. Chen, T. Zhang, K. Lu, and C. K. Chan, Phys. Rev. Lett. **91**, 204301 (2003).
[14] K. Huang, M. Brinkmann, and S. Herminghaus, Soft Matter **8**, 11939 (2012).
[15] M. Hou, H. Tu, R. Liu, Y. Li, K. Lu, P. Y. Lai, and C. K. Chan, Phys. Rev. Lett. **100**, 068001 (2008).
[16] Y. Li, R. Liu, and M. Hou, Phys. Rev. Lett. **109**, 198001 (2012).
[17] P. Jop, Y. Forterre, and O. Pouliquen, Nature (London) **441**, 727 (2006).
[18] R. Delannay, M. Louge, P. Richard, N. Taberlet, and A. Valance, Nat. Mater. **6**, 99 (2007).
[19] W. A. Beverloo, H. A. Leniger, and J. van de Velde, Chem. Eng. Sci. **15**, 260 (1961).
[20] A. Janda, I. Zuriguel, and D. Maza, Phys. Rev. Lett. **108**, 248001 (2012).
[21] C. Mankoc, A. Janda, A. Arevalo, J. M. Pastor, I. Zuriguel, A. Garcimartín, and D. Maza, Granular Matter **9**, 407 (2007).
[22] J. J. Drozd and C. Denniston, Phys. Rev. E **78**, 041304 (2008).
[23] A. Tripathi and D. V. Khakhar, Phys. Rev. E **81**, 041307 (2010).
[24] V. Kumaran and S. Maheshwari, Phys. Fluids **24**, 053302 (2012).
[25] G. C. Yang, Q. Y. Liu, M. B. Hu, R. Jiang, and Q. S. Wu, Phys. Lett. A **378**, 1281 (2014).
[26] M. B. Hu, Q. Y. Liu, W. P. Sun, R. Jiang, and Q. S. Wu, Appl. Math. Mech. (Engl. Ed.) **35**, 1565 (2014).
[27] G. C. Yang, Q. Y. Liu, M. B. Hu, R. Jiang, Q. S. Wu, and R. Wang, Appl. Mech. Mater. **487**, 400 (2014).
[28] R. Jiang, Q. S. Wu, and B. H. Wang, Phys. Rev. E **66**, 036104 (2002).
[29] B. S. Kerner, *Introduction to Modern Traffic Flow Theory and Control: The Long Road to Three-Phase Traffic Theory* (Springer, Berlin, 2009).
[30] D. Helbing, Rev. Mod. Phys. **73**, 1067 (2001).